Deubiquitinating enzyme CYLD negatively regulates RANK signaling and osteoclastogenesis in mice

Wei Jin,[1,2] Mikyoung Chang,[1,2] Emmanuel M. Paul,[3] Geetha Babu,[2] Andrew J. Lee,[1,2] William Reiley,[1] Ato Wright,[1,2] Minying Zhang,[1] Jun You,[3] and Shao-Cong Sun[1]

[1]Department of Immunology, The University of Texas MD Anderson Cancer Center, Houston, Texas, USA. [2]Department of Microbiology and Immunology and [3]Department of Orthopaedics and Rehabilitation, Pennsylvania State University College of Medicine, Hershey, Pennsylvania, USA.

Osteoclastogenesis is a tightly regulated biological process, and deregulation can lead to severe bone disorders such as osteoporosis. The regulation of osteoclastic signaling is incompletely understood, but ubiquitination of TNF receptor–associated factor 6 (TRAF6) has recently been shown to be important in mediating this process. We therefore investigated the role of the recently identified deubiquitinating enzyme CYLD in osteoclastogenesis and found that mice with a genetic deficiency of CYLD had aberrant osteoclast differentiation and developed severe osteoporosis. Cultured osteoclast precursors derived from CYLD-deficient mice were hyperresponsive to RANKL-induced differentiation and produced more and larger osteoclasts than did controls upon stimulation. We assessed the expression pattern of CYLD and found that it was drastically upregulated during RANKL-induced differentiation of preosteoclasts. Furthermore, CYLD negatively regulated RANK signaling by inhibiting TRAF6 ubiquitination and activation of downstream signaling events. Interestingly, we found that CYLD interacted physically with the signaling adaptor p62 and thereby was recruited to TRAF6. These findings establish CYLD as a crucial negative regulator of osteoclastogenesis and suggest its involvement in the p62/TRAF6 signaling axis.

Introduction

Normal bone physiology is regulated by the harmonic actions of osteoblasts and osteoclasts (OCs), cells that mediate bone formation and bone resorption, respectively (1). OCs are multinucleated cells that are derived from macrophage precursors. OC differentiation is induced by RANKL in the presence of the macrophage growth factor M-CSF (2, 3). Binding of RANKL to its receptor, RANK, stimulates receptor trimerization and recruitment of signaling adaptors, most importantly TNF receptor–associated factor 6 (TRAF6) (4). TRAF6 transduces the RANK-mediated signal by initiating a number of downstream signaling pathways, including those that activate the transcription factors NF-κB and activator protein 1 (AP-1) (4, 5). These transcription factors in turn induce the expression of a master osteoclastogenic regulator, nuclear factor of activated T cells c1 (NFATc1), and trigger a cascade of gene expression events required for OC differentiation (3, 5, 6). Genetic deficiencies in TRAF6 or its downstream signaling factors attenuate OC differentiation and bone resorption, a condition known as osteopetrosis (3, 7). On the other hand, excessive production or activation of OCs can lead to uncontrolled bone resorption or osteoporosis. Thus, a fundamental understanding of RANK signaling is important for rational design of therapeutic approaches for the treatment of bone disorders.

Recent studies suggest that ubiquitination of TRAF6 is an important mechanism mediating its signaling functions (8–10). Lysine 63–linked polyubiquitin chains facilitate the association of TRAF6 with target signaling factors, such as IκB kinase (IKK), a multisubunit enzyme mediating activation of NF-κB (11). The regulatory subunit of IKK, IKKγ (also known as NEMO), has intrinsic ubiquitin-binding activity and is thought to recruit the IKK catalytic subunits, IKKα and IKKβ, to ubiquitinated upstream regulators (12, 13). How the ubiquitination and signaling function of TRAF6 are regulated under physiological conditions, particularly during osteoclastogenesis, is incompletely understood. Nevertheless, an adaptor protein, p62 (also known as sequestosome 1), has been shown to physically associate with TRAF6 and play both positive and negative roles in RANK signaling. Complete loss of p62 attenuates RANK signaling and osteoclastogenesis (14). On the other hand, mutations of p62 that disrupt its C-terminal ubiquitin association (UBA) domain cause aberrant RANK signaling and hyperproduction of OCs (3, 15–18). Such genetic alterations of p62 are etiologically associated with development of Paget disease of bone (PDB), a severe bone disorder characterized by formation of giant OCs, excessive bone resorption, and irregular bone formation (15, 19, 20). The positive signaling role of p62 appears to involve recruitment of atypical PKCs to TRAF6, which contributes to IKK activation by RANK (14). Although how p62 negatively regulates RANK signaling is unclear, one implication is that p62 may be involved in interaction with negative regulators.

An emerging family of signaling regulators involved in diverse biological processes are deubiquitinating enzymes (DUBs), which digest ubiquitin chains and reverse the process of protein ubiquitination (21). One DUB, CYLD, has been implicated as an important regulator of immune response and oncogenesis (22–28). The signaling function of CYLD appears to be cell type specific. Thus, CYLD negatively regulates the activation of IKK and JNK in lymphocytes but has no obvious role in regulating these signal-

Nonstandard abbreviations used: AP-1, activator protein 1; BMDM, bone marrow–derived macrophage; DUB, deubiquitinating enzyme; IKK, IκB kinase; M-CSFR, M-CSF receptor; microCT, microcomputed tomography; NFATc1, nuclear factor of activated T cells c1; NIK, NF-κB–inducing kinase; OC, osteoclast; PDB, Paget disease of bone; TRAF6, TNF receptor–associated factor 6; TRAP, tartrate-resistant acid phosphatase; UBA, ubiquitin association.

Conflict of interest: The authors have declared that no conflict of interest exists.

Citation for this article: *J. Clin. Invest.* **118**:1858–1866 (2008). doi:10.1172/JCI34257.

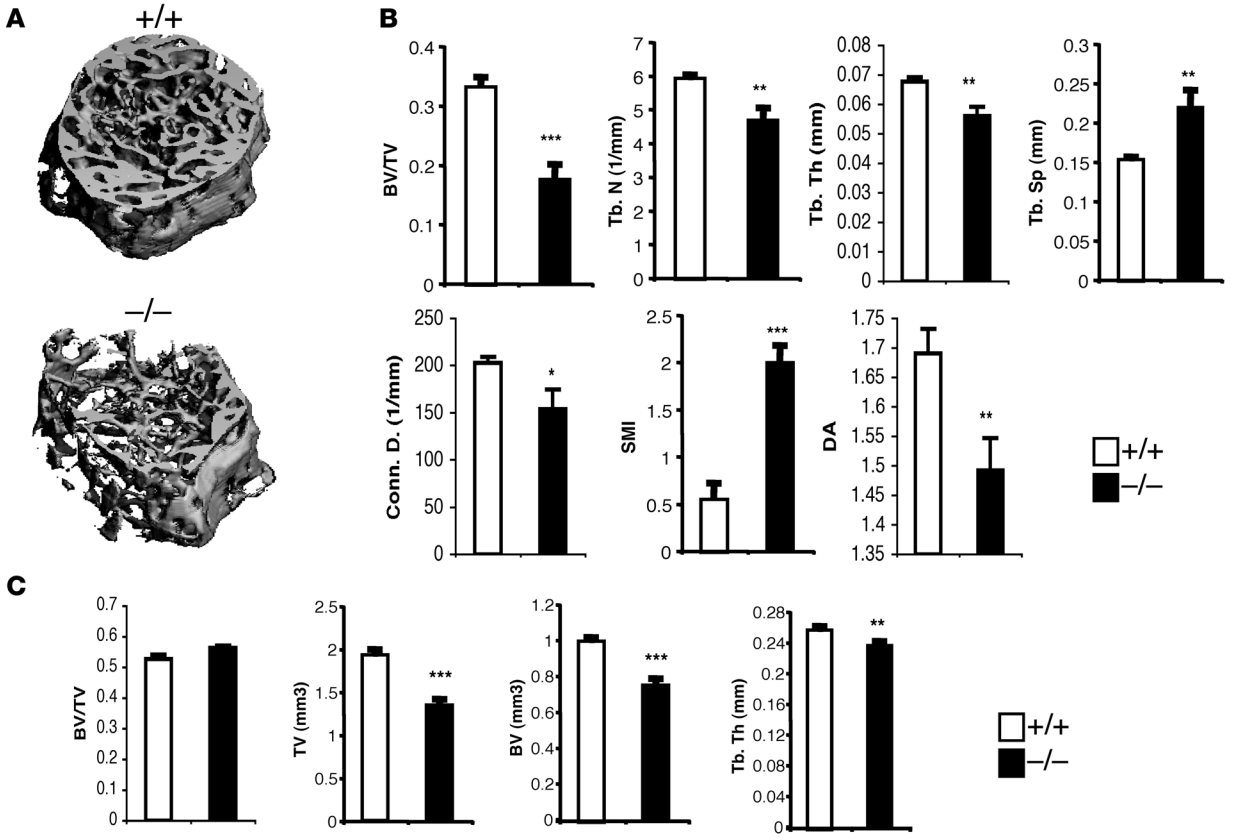

Figure 1
Bone loss in *Cyld*$^{-/-}$ mice. Age-matched *Cyld*$^{+/+}$ and *Cyld*$^{-/-}$ male mice (14 weeks of age, 7 per group) were subjected to microCT analysis. (**A**) Representative images of 3D microCT reconstruction of trabecular bone 263 μm above the distal femoral growth plate showing the severe bone loss in *Cyld*$^{-/-}$ mice. (**B**) Parameters of trabecular bone mass, including bone volume fraction (BV/TV), trabecular number (Tb. N), trabecular thickness (Tb. Th), trabecular separation (Tb. Sp), connectivity density (Conn. D), structure model index (SMI), and degree of anisotropy (DA). (**C**) Parameters of cortical bone mass, including bone volume fraction, total volume (TV), bone volume (BV), and cortical bone thickness (Tb. Th). **P* < 0.05, ***P* < 0.02, ****P* < 0.002. Error bars represent SEM.

ing events in macrophages (22–24). In the present study, we show that the expression level of CYLD is extremely low in macrophages but is markedly upregulated under conditions of RANKL-induced osteoclastogenesis. We provide genetic evidence that CYLD is a crucial negative regulator of RANK signaling in preosteoclasts. The loss of CYLD in mice causes production of enlarged and hypernucleated OCs, associated with severe osteoporosis. Interestingly, the adaptor protein p62 physically interacts with CYLD and promotes the binding of CYLD to TRAF6, and this novel molecular interplay requires the C-terminal region of p62. These findings establish CYLD as what we believe to be the first DUB that regulates osteoclastogenesis and suggest a potential mechanism mediating the negative signaling function of p62.

Results

Cyld-knockout mice develop osteoporosis. To investigate the physiological functions of CYLD, we generated *Cyld*-knockout mice (22). During the preparation of bone marrow cells, we noticed that the femurs of *Cyld*-knockout (*Cyld*$^{-/-}$) mice appeared to be more fragile than those of wild-type mice. This finding prompted us to compare the bone mass and structure of *Cyld*$^{-/-}$ and wild-type (*Cyld*$^{+/+}$) mice. Femurs of *Cyld*$^{+/+}$ and *Cyld*$^{-/-}$ mice were subjected to microcomputed tomography (microCT) analyses. The *Cyld*$^{-/-}$ mice exhibited severe loss of trabecular bone, as shown in representative images of 3D microCT reconstruction (Figure 1A). Consistently, the volume of trabecular bone per unit of metaphysis (BV/TV) was reduced by almost half in the *Cyld*$^{-/-}$ mice (Figure 1B). The mutant animals also displayed obvious abnormalities in several other parameters of trabecular bone architecture, including decreased trabecular number and trabecular thickness (Tb. Th), but increased trabecular separation, which together suggested a reduced and more separated trabecular bone network. Structure model index is scored from 0 to 3 for indication of increased fragility. Compared with wild-type femurs, the *Cyld*$^{-/-}$ femurs had dramatically higher SMI numbers and lower degree of anisotropy and connectivity density, indicating more fragile bone in the mutant animals (Figure 1B). In agreement with the trabecular bone data, analysis of the cortical bone at the midshaft level revealed a moderate but significant decrease in cortical bone thickness (Figure 1C, Tb. Th). The total volume (TV) of cortical bone and the volume of bone fraction (BV) were also reduced. However, the proportion of bone (BV/TV) remained the same in wild-type and *Cyld*$^{-/-}$ femurs, indicating decreased diameter

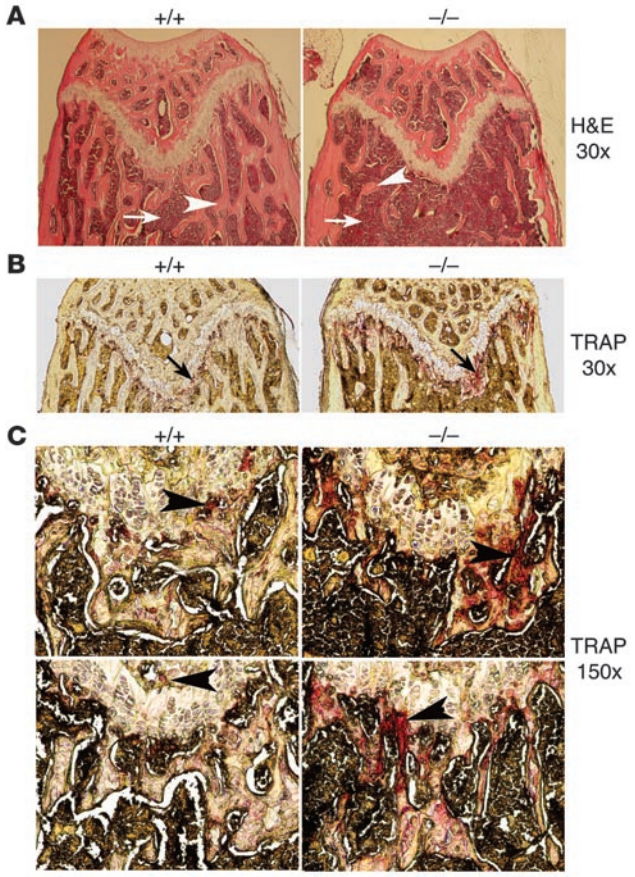

Figure 2
Cyld$^{-/-}$ mice have enlarged OCs. (**A**) H&E staining of femoral sections of age-matched *Cyld*$^{+/+}$ and *Cyld*$^{-/-}$ mice (14 weeks old), showing reduced trabecular bone (white arrowheads) in *Cyld*$^{-/-}$ femur. White arrows indicate bone marrow. (**B**) Increased TRAP activity in *Cyld*$^{-/-}$ bone compared with *Cyld*$^{+/+}$ (black arrows). Original magnification, ×30. (**C**) Higher-magnification (×150) images showing the enlarged TRAP-positive OCs in 2 different *Cyld*$^{+/+}$ and *Cyld*$^{-/-}$ mice.

of *Cyld*$^{-/-}$ femurs but not defect in osteoblast function. These results suggest that the loss of CYLD in mice leads to osteoporosis.

Cyld$^{-/-}$ *mice exhibit OC abnormalities*. To address the mechanism by which CYLD regulates bone density, we performed histological analyses of femurs from *Cyld*$^{+/+}$ and *Cyld*$^{-/-}$ mice. Consistent with the microCT results, H&E staining of femoral sections revealed a severe reduction in trabecular bone in *Cyld*$^{-/-}$ mice (Figure 2A). Moreover, the *Cyld*$^{-/-}$ trabecular bone contained increased OC activity, as revealed by positive staining with tartrate-resistant acid phosphatase (TRAP) (Figure 2B). Additionally, the OCs from *Cyld*$^{-/-}$ mice were markedly enlarged in size (Figure 2C). On the other hand, bone nodule assays to test the ability of osteoblasts to form mineralized bone in vitro did not show obvious difference between the *Cyld*$^{-/-}$ and wild-type mice (Supplemental Figure 1A; supplemental material available online with this article; doi:10.1172/JCI34257DS1). Furthermore, the *Cyld*$^{-/-}$ mice only had a weak increase in serum concentration of osteocalcin, an indicator of osteoblast activity (Supplemental Figure 1B). Thus, as seen with mice expressing a p62 mutant (18), the *Cyld*$^{-/-}$ mice have abnormalities predominantly in OCs, leading to osteoporosis.

CYLD negatively regulates osteoclastogenesis. The OC abnormalities in *Cyld*$^{-/-}$ mice led us to examine the role of CYLD in regulating OC differentiation. Bone marrow–derived macrophages (BMDMs) were cultured in M-CSF growth medium in either the absence or presence of RANKL. As expected, RANKL induced the generation of TRAP-positive OCs at a concentration of 100 ng/ml (Figure 3A). Remarkably, the same concentration of RANKL induced a drastically higher number of OCs in the *Cyld*$^{-/-}$ BMDMs (Figure 3A). The *Cyld*$^{-/-}$ OCs were also notably larger (Figure 3A) and contained substantially more nuclei than the control OCs (Figure 3B). A dose-response assay revealed that loss of CYLD also rendered the cells responsive to lower doses of RANKL (Figure 3C). These results were not due to alteration in the surface expression of RANK (Supplemental Figure 2). The level of M-CSF receptor (M-CSFR) was also similar in the wild-type and *Cyld*$^{-/-}$ cells (Supplemental Figure 2). Consistent with these results, overexpression of CYLD in wild-type OC precursor cells strongly inhibited the osteoclastogenesis (Supplemental Figure 3).

We next performed real-time PCR to examine the effect of *Cyld* deficiency on the induction of osteoclastogenic markers, including the early markers TRAP and cathepsin K and the late marker calcitonin receptor. Following RANKL stimulation, the expression of TRAP and cathepsin K was increased within 1–2 days, whereas the induction of calcitonin receptor occurred at 2–3 days (Figure 3D). Importantly, induction of both the early and late osteoclastogenic markers was greatly potentiated in *Cyld*$^{-/-}$ cells (Figure 3D). Together, these results suggest a crucial role for CYLD in negatively regulating osteoclastogenesis.

CYLD negatively regulates RANK signaling in preosteoclasts. To elucidate the molecular mechanism by which CYLD negatively regulates osteoclastogenesis, we examined the effect of *Cyld* deficiency on RANKL-stimulated signaling events. Stimulation of wild-type BMDMs with RANKL resulted in rapid activation of MAPKs, including ERK, JNK, and p38 (Figure 4A) as well as NF-κB (Figure 4B). The *Cyld* deficiency had no obvious effect on the early activation of MAPKs (Figure 4A). Similarly, during the initial phase of RANKL stimulation in BMDMs, the loss of CYLD did not substantially affect the activation of NF-κB (Figure 4B). Another transcription factor, AP-1, was not detected under the short-term stimulation conditions (data not shown). Thus, CYLD is not involved in regulation of the initial phase of RANK signaling in BMDMs.

We next examined the role of CYLD in RANK signaling in developing OCs, hereafter referred to preosteoclasts. Active NF-κB and AP-1 were detected in the nuclei of preosteoclasts exposed to RANKL for 2 days (Figure 4C). Interestingly, the activity of both NF-κB and AP-1 was markedly enhanced in *Cyld*$^{-/-}$ cells. Recent studies suggest that OC development involves induction of NFATc1, a master regulator of osteoclastogenesis (5, 29). Since NF-κB and AP-1 have been implicated in the induction of NFATc1, we examined whether the loss of CYLD also promoted NFATc1 induction. Indeed, substantially higher levels of NFATc1 were induced by RANKL in *Cyld*$^{-/-}$ cells than in the control cells (Figure 4D). On the other hand, the loss of CYLD did not affect the induction of TRAF6 or constitutive expression of the protein kinase Tak1 (Figure 4D). These results suggest that CYLD regulates the sustained activation of NF-κB and AP-1 and induction of NFATc1 in preosteoclasts, which provides a molecular insight into the role of CYLD in regulating osteoclastogenesis.

Induction of CYLD expression under conditions of OC differentiation. Because of the distinct roles of CYLD in BMDMs and preosteoclasts, we examined its expression pattern under conditions of

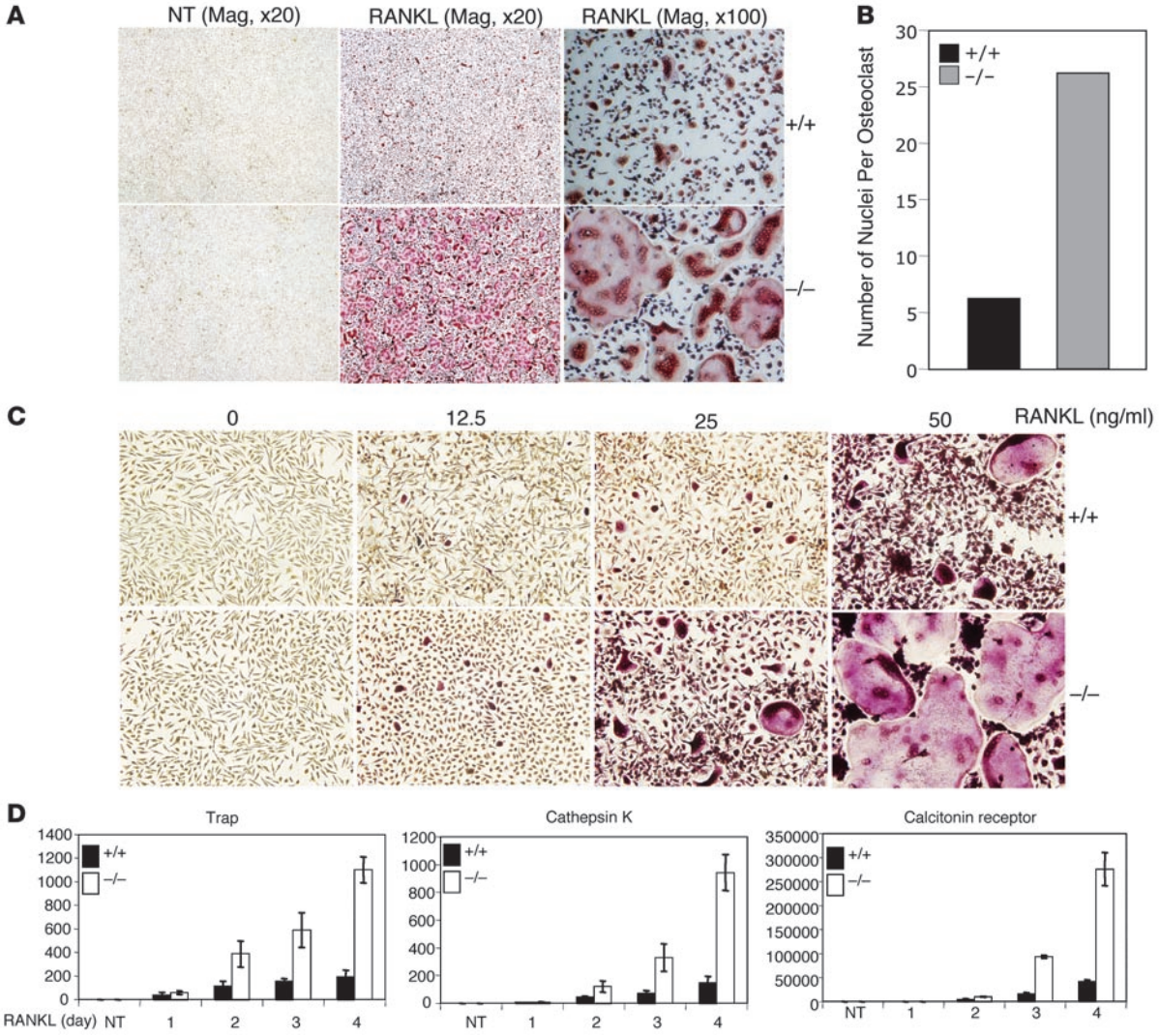

Figure 3

Enhanced OC differentiation from *Cyld*$^{-/-}$ bone marrow cells. (**A**) Bone marrow cells derived from age-matched *Cyld*$^{+/+}$ and *Cyld*$^{-/-}$ mice were cultured in M-CSF media either in the absence (NT) or presence of 100 ng/ml of GST-RANKL for 4 days and then subjected to TRAP staining. The images of RANKL-stimulated cells are presented as lower (×20) and higher (×100) magnifications. (**B**) Average number of nuclei per OC calculated based on counting in 15 *Cyld*$^{+/+}$ and 15 *Cyld*$^{-/-}$ OCs. (**C**) Bone marrow cells derived from CYLD$^{+/+}$ and CYLD$^{-/-}$ mice were cultured in M-CSF media supplemented with the indicated amounts of GST-RANKL. After 7 days, OCs were detected by TRAP staining. Note that this experiment used a longer differentiation time (7 days) than that shown in Figure 3A in order to detect OCs in the wild-type cell culture at low doses of GST-RANKL. (**D**) Real-time RT-PCR was performed using RNA isolated from BMDMs or BMDMs cultured in the presence of both M-CSF and 100 ng/ml GST-RANKL for the indicated times. The relative mRNA level of individual genes was expressed as fold induction compared with NT *Cyld*$^{+/+}$ cells. Data represent mean values of 3 independent experiments, with error bars indicating SD.

RANKL-induced OC differentiation. Consistent with its dispensable role during the early phase of RANK signaling, the level of CYLD was extremely low in BMDMs (Figure 5A). Interestingly, CYLD expression was markedly increased after 1 day of RANKL stimulation and further upregulated after prolonged stimulation (Figure 5A and data not shown). The RANKL-induced upregulation of CYLD protein was associated with induction of *Cyld* mRNA, as determined by parallel real-time PCR assays (Figure 5B). This pattern of CYLD expression provides a good explanation for its specific signaling function in preosteoclasts.

Since RANKL stimulates rapid activation of both canonical NF-κB and MAPKs in BMDMs, the delayed induction of CYLD expression suggested the requirement of additional regulators. As an initial approach to address this issue, we examined whether CYLD expression is also induced by other macrophage inducers, including the bacterial endotoxin LPS and the proinflammatory cytokine TNF-α. In contrast to RANKL, neither TNF-α nor LPS substantially increased the expression of CYLD (Figure 5C). On the other hand, LPS potently increased the expression of a known proinflammatory mediator, iNOS, and both TNF-α and LPS induced the expression of the *Nfkb2* gene product p100 (Figure 5C). Thus, the induction of CYLD appeared to be specifically mediated by the OC inducer RANKL.

An important feature of RANKL-stimulated signaling is the induction of noncanonical NF-κB (30), a process that is regulated

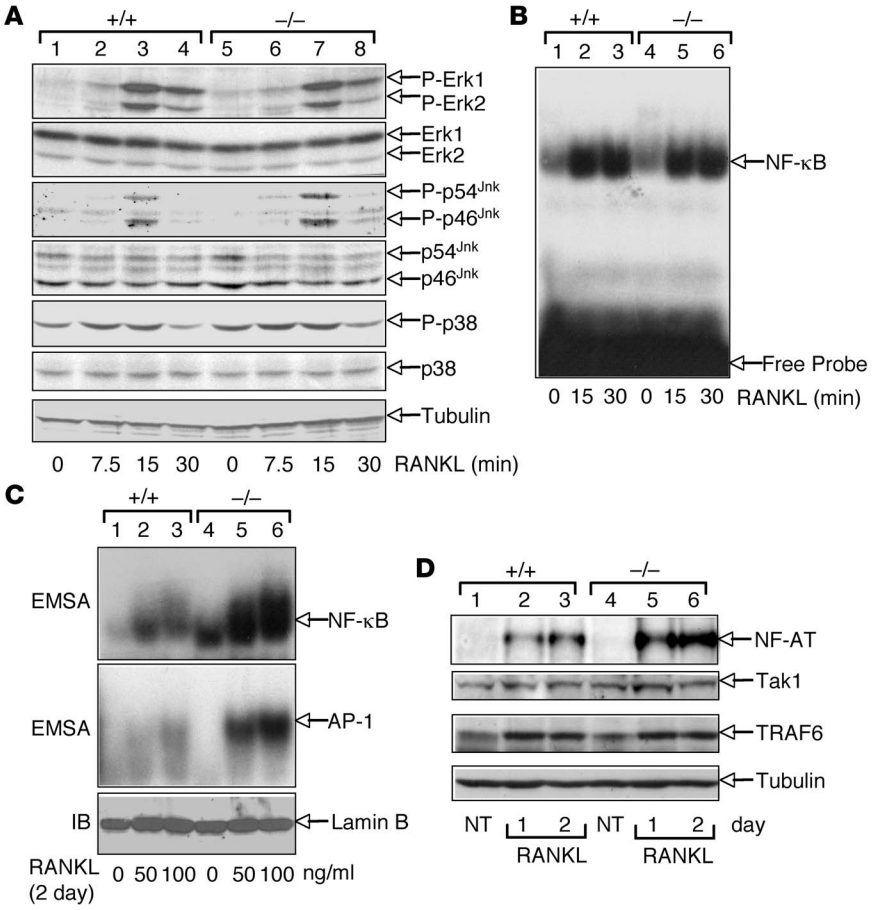

Figure 4
RANK signaling is normal in BMDMs but aberrant in preosteoclasts in the absence of CYLD. (**A**) BMDMs were cultured in M-CSF–containing medium and stimulated with GST-RANKL (100 ng/ml) for the indicated times and subjected to IB assays using phospho-specific (P-) or regular antibodies against the indicated MAPKs or tubulin. (**B**) BMDMs were stimulated with GST-RANKL for the indicated times as in **A**, and the nuclear NF-κB DNA binding activity was detected by EMSA. (**C**) BMDMs were cultured for 2 days in M-CSF medium lacking (represented by 0) or containing the indicated amounts of GST-RANKL. Nuclear extracts were subjected to EMSA to detect the activation of NF-κB or AP-1. An IB of lamin B was included as a loading control. (**D**) BMDMs were cultured in M-CSF medium for 2 days in the absence of RANKL (NT) or for the indicated days in the presence of RANKL. Total cell lysates were subjected to IB to detect the indicated proteins.

by NF-κB–inducing kinase (NIK) and involves processing of the NF-κB2 precursor protein p100 to generate p52 (31). To examine the involvement of noncanonical NF-κB in CYLD induction, we examined RANKL-stimulated expression of CYLD in *Nik*$^{-/-}$ and control BMDMs. As expected, RANKL stimulated the processing of p100 (generation of p52) in wild-type but not *Nik*$^{-/-}$ cells (Figure 5D). Interestingly, the RANKL-induced expression of CYLD was severely attenuated, although not completely blocked, in *Nik*$^{-/-}$ cells. Thus, optimal induction of CYLD by RANKL requires the noncanonical NF-κB signaling pathway, which may function in cooperation with the canonical NF-κB and other signaling pathways.

CYLD is assembled into the TRAF6 complex and negatively regulates TRAF6 ubiquitination in preosteoclasts. TRAF6 is a master signaling molecule controlling multiple downstream pathways induced by RANKL. Ubiquitination of TRAF6 plays an important role in its signaling function, including the regulation of osteoclastogenesis (8–10). The finding that CYLD negatively regulates RANK signaling and osteoclastogenesis prompted us to examine whether the loss of CYLD altered ubiquitination of TRAF6 in preosteoclasts. As expected, polyubiquitinated TRAF6 was detected in RANKL-induced preosteoclasts (Figure 6A). Importantly, substantially more ubiquitinated TRAF6 was accumulated in *Cyld*$^{-/-}$ cells (Figure 6A). Moreover, the TRAF6 ubiquitination in *Cyld*$^{-/-}$ cells was more persistent than in *Cyld*$^{+/+}$ cells, as revealed when the cells were chased in RANKL-free media (Figure 6A, lanes 5 and 6). Consistent with these results, transfected CYLD potently inhibited RANK-induced TRAF6 ubiquitination (Supplemental Figure 4). Thus, CYLD plays a nonredundant role in suppressing the ubiquitination of TRAF6 during RANKL-induced OC differentiation, a finding that provides an insight into the molecular mechanism by which CYLD regulates osteoclastogenesis.

We next examined the physical association between CYLD and TRAF6. The expression level of both CYLD and TRAF6 was upregulated in RANKL-induced preosteoclasts (Figure 6B, middle and bottom panels). Moreover, TRAF6 and CYLD were coprecipitated (Figure 6B, top panel), indicating their presence in the same complex. Together, these results emphasize a physiological role of CYLD in negatively regulating TRAF6 ubiquitination mediated by RANKL.

p62 physically interacts with CYLD and promotes the CYLD/TRAF6 association. Prior studies have identified p62 as a component of the TRAF6 complex during osteoclastogenesis (14). Like CYLD, p62 is markedly induced during RANKL-stimulated OC differentiation (Figure 6C and ref. 14). Since p62 is known as an adaptor of TRAF6, we examined whether CYLD was physically associated with p62. Indeed, a stable complex of p62 and CYLD was readily identified from preosteoclasts by coimmunoprecipitation assays (Figure 6C). The p62/CYLD interaction was also demonstrated using transfected 293 cells (Figure 6D). Interestingly, a p62 mutant lacking its C-terminal UBA domain (p62ΔUBA) was largely defective in CYLD binding (Figure 6D). This phenotype of p62ΔUBA was not due to the variation in its expression, since this mutant was expressed at even higher levels than the wild-type p62.

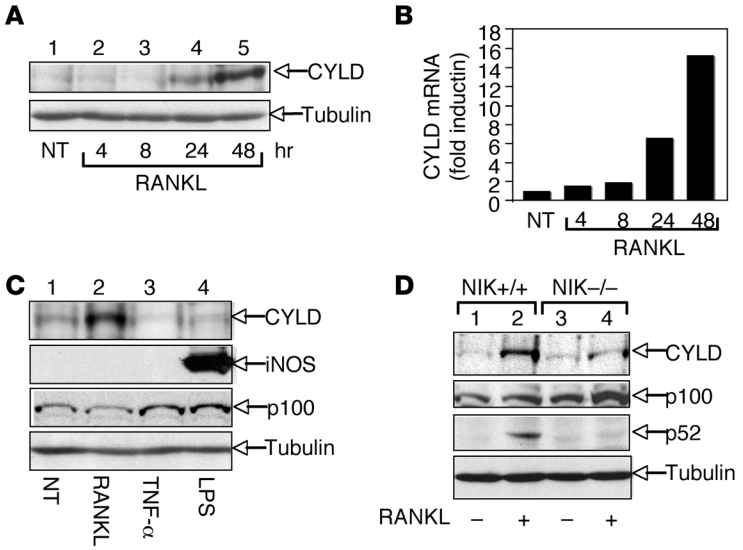

Figure 5
Induction of CYLD expression by RANKL but not by LPS or TNF-α. (**A**) Wild-type BMDMs were cultured in M-CSF–containing medium in the absence of RANKL (NT) or for the indicated times in the presence of GST-RANKL (100 ng/ml). Total cell lysates were subjected to IB to detect CYLD and tubulin. (**B**) Real-time RT-PCR was performed using RNA isolated from cells as described in **A** to determine the relative expression of *Cyld* mRNA. (**C**) Wild-type BMDMs were cultured in M-CSF medium for 1 day in either the absence (NT) or presence of the indicated inducers. Total cell lysates were subjected to IB to detect the indicated proteins. (**D**) BMDMs prepared from *Nik*-knockout (NIK–/–) and control (NIK+/+) mice were cultured for 1 day in the absence (–) or presence (+) of GST-RANKL (100 ng/ml) followed by IB to detect the expression of CYLD (top panel) or processing of p100 (middle 2 panels). A tubulin IB was used as a loading control.

The strong interaction of p62 with CYLD led us to examine whether p62 facilitates the assembly of CYLD into the TRAF6 complex. We found that in 293 cells, endogenous TRAF6 did not appreciably associate with CYLD (Figure 6E, top panel, lane 2), a finding that was consistent with a previous report (32). Remarkably, however, expression of p62 in the cells induced the complex formation between CYLD and TRAF6 (Figure 6E, top panel, lane 3, and Supplemental Figure 5). Furthermore, this function of p62 was correlated with its CYLD-binding activity, since it was not seen with the p62ΔUBA mutant (lane 4). Thus, p62 appears to function as an adaptor recruiting CYLD to TRAF6, thus providing a molecular insight into the negative function of p62 in osteoclastogenesis. On the other hand, the association of p62 with TRAF6 was not affected by CYLD (Supplemental Figure 6). CYLD was also not involved in RANK-mediated activation of PKCζ (Supplemental Figure 6), which is thought to involve the positive signaling function of p62. These findings suggest that CYLD may specifically mediate the negative signaling function of p62 by deubiquitinating TRAF6.

Discussion

Osteoclastogenesis is a tightly controlled biological process that involves both positive and negative regulation. Compared with the positive players, the negative regulators of this process are relatively less well understood. Prior studies have identified the suppressive role of SHIP-1 and IRAK-M in OC formation. Both proteins are abundantly expressed in macrophages, the OC precursors, and have inhibitory roles in innate immune signaling (33, 34). SHIP-1 controls osteoclastogenesis by targeting M-CSFR signaling, while IRAK-M acts by inhibiting the IL-1 receptor pathway (35–37). Our present study suggests that CYLD, unlike SHIP-1 or IRAK-M, functions as a specific negative regulator of OC development by suppressing RANK signaling.

We have previously shown that loss of CYLD in macrophages has no obvious effect on the signaling events mediated by innate immune stimuli, such as TNF-α and LPS (22, 24). Similarly, we have found in the present study that CYLD does not regulate RANKL-stimulated initial signaling in BMDMs. In sharp contrast, CYLD has a crucial role in controlling RANKL-stimulated signaling in preosteoclasts. This functional diversity of CYLD is likely due to its differential expression. The level of CYLD is very low in BMDMs, but it is drastically upregulated in preosteoclasts. Interestingly, the induction of CYLD expression is specific for RANKL signal, as it is not seen with the proinflammatory stimuli TNF-α and LPS, which potentially explains the functional specificity of CYLD in RANK signaling. Although how RANKL specifically induces the expression of CYLD is incompletely understood, our data suggest the requirement of a noncanonical NF-κB signaling pathway. Thus, as depicted in Figure 7, we believe *Cyld* to be a novel target gene of RANK signaling that is involved in the feedback inhibition.

The expression pattern of CYLD is reminiscent of that of p62 (14), a signaling adaptor with positive and negative roles in regulating osteoclastogenesis. p62 physically associates with TRAF6 and appears to promote RANK signaling by recruiting atypical PKCs to TRAF6 (14). Under overexpression conditions, p62 also induces the self-ubiquitination activity of TRAF6, although the physiological relevance remains unclear (38). How p62 negatively regulates RANK signaling has remained poorly understood, although this function of p62 is known to require its C-terminal region (3, 15–18). Our present study shows that p62 physically interacts with CYLD and promotes the binding of CYLD to TRAF6. CYLD is assembled into the TRAF6 complex and plays an essential role in preventing excessive ubiquitination of TRAF6 in preosteoclasts. Moreover, the C-terminal region of p62 is essential for its adaptor function to promote CYLD/TRAF6 interaction. These findings suggest an intriguing molecular interplay between p62 and CYLD and shed light on how p62 negatively regulates RANK signaling (Figure 7).

A recent study demonstrates that transgenic mice expressing a mutated form of p62 develop osteoporosis, although the p62 mutation is insufficient to cause the full PDB phenotype (18). In particular, the p62 mutation causes abnormal osteoclastogenesis but does not enhance osteoblast numbers and activity, as seen in PDB. These findings suggest that p62 mutations may predispose individuals to, but be insufficient for, the development of PDB. Our data indicate that CYLD may mediate an important part of the negative signaling functions of p62. As seen with the p62-mutant transgenic mice, *Cyld*$^{-/-}$ mice spontaneously develop osteoporosis, although they do not show significant abnormalities in osteoblast development and function. Our in vitro studies

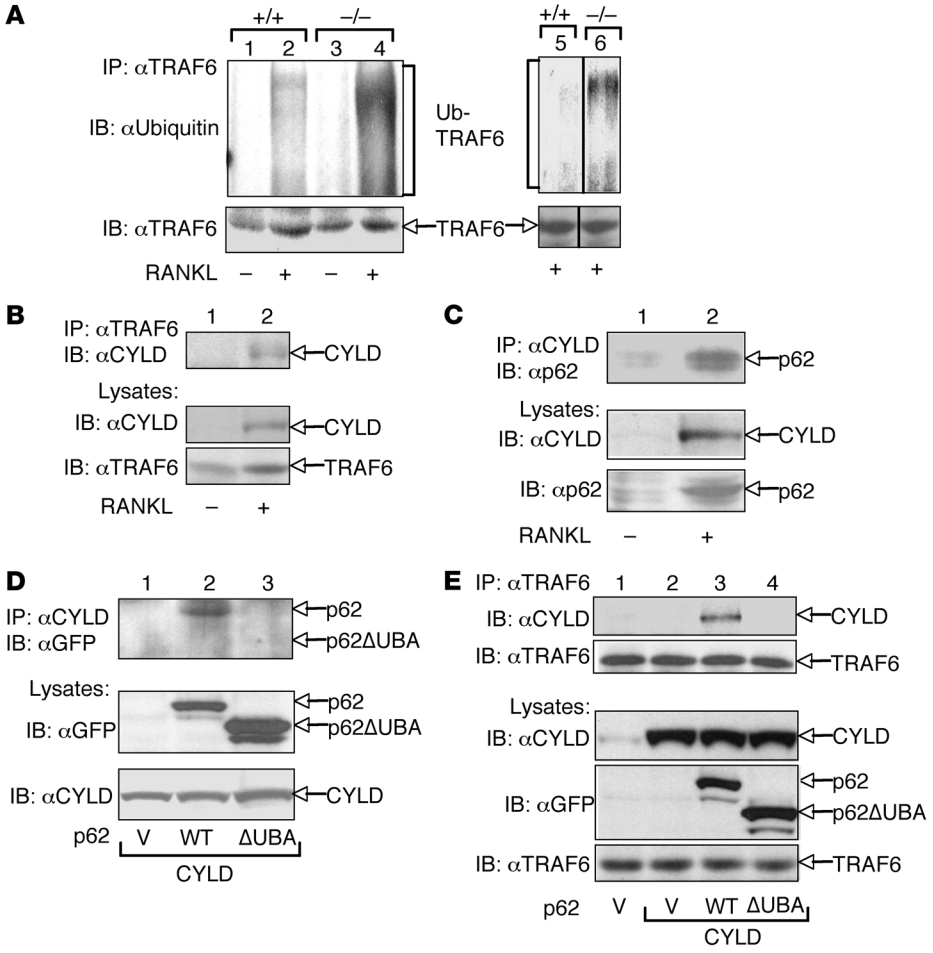

Figure 6

CYLD targets TRAF6, which is promoted by p62. (**A**) Wild-type and *Cyld*$^{-/-}$ BMDMs were cultured for 2 days in M-CSF medium in either the absence (–) or presence (+) of GST-RANKL. TRAF6 was isolated by IP followed by IB to detect ubiquitin-conjugated TRAF6 (upper panel) or unmodified TRAF6 (lower panel). In lanes 5 and 6, the RANKL-treated cells were chased in RANKL-free media overnight before the TRAF6 ubiquitination assay. (**B**) Wild-type BMDMs were cultured for 2 days in M-CSF medium in the absence or presence of GST-RANKL. TRAF6 was isolated by IP followed by detection of the associated CYLD by IB (top panel). The lysates were subjected to IB to monitor the expression of CYLD and TRAF6 (middle and bottom panels). (**C**) Wild-type BMDMs were cultured for 2 days in M-CSF medium in the absence or presence of GST-RANKL. CYLD was isolated by IP followed by detection of the associated p62 by IB (top panel). The cell lysates were subjected to IB to monitor the expression of CYLD and p62 (middle and bottom panels). (**D**) 293 cells were transfected with CYLD along with vector control (V), wild-type p62, or p62ΔUBA. CYLD was isolated by IP, and its associated p62 was detected by IB (top panel). Protein expression in cell lysates was monitored by direct IB (middle and bottom panels). (**E**) 293T cells were transfected with either an empty vector or expression vectors encoding wild-type p62 or p62ΔUBA. Lanes 2–4 were also transfected with CYLD. Endogenous TRAF6 was isolated by IP followed by IB to detect the associated CYLD or the precipitated TRAF6 (top 2 panels). The cell lysates were subjected to IB to detect the expression of CYLD, EGFP-tagged p62 proteins, and TRAF6 (bottom 3 panels).

further reveal that the *Cyld* deficiency strongly promotes osteoclastogenesis, causing the formation of increased numbers of large and multinucleated OCs. These phenotypes are associated with aberrant RANK signaling. It is likely that the enhanced RANK signaling in *Cyld*$^{-/-}$ cells promotes formation of mononuclear preosteoclasts, which in turn fuse to form the multinucleated OCs. Since larger OCs have been reported in diseases associated with excessive bone resorption, such as PDB, our present study suggests CYLD as a potential genetic factor involved in the development of bone disorders.

Methods

Mice. *Cyld*-knockout mice were generated as described previously (22). Heterozygous (*Cyld*$^{+/-}$) mice were intercrossed to generate *Cyld*$^{-/-}$ and *Cyld*$^{+/+}$ littermates, and genotyping was performed by PCR using tail DNA (24). *Nik*-knockout mice were provided by Amgen Inc. All mice were housed in specific pathogen–free cages and monitored periodically (every 3 months) for the lack of common pathogens. Animal experiments were performed in accordance with protocols approved by the Pennsylvania State University College of Medicine Institutional Animal Care and Use Committee.

Plasmids, antibodies, and reagents. Expression vectors encoding pEGFP-p62 and pEGFP-p62ΔUBA were provided by Jiake Xu (University of Western Australia, Nedlands, Western Australia, Australia) and described previously (16), and the expression vectors for FLAG-tagged p62 and FLAG-tagged RANK were provided by Gregory D. Longmore (Washington University, St. Louis, Missouri, USA) and Yongwon Choi (University of Pennsylvania, Philadelphia, Pennsylvania, USA). pCLXSN(GFP), pCLXSN(GFP)-CYLD, pcDNA-HA-CYLD, and pcDNA-HA-CYLD 1-932 (a catalytically inactive mutant) were described previously (39, 40). PE-conjugated anti-mouse RANK (clone IK22/5) and anti-mouse M-CSFR (CD115, clone AFS98) were from eBioscience. Antibodies against iNOS (M-19), TRAF6 (H274), lamin B (H-90), p62 (SQSTM 1, D-3), anti-PKCζ (C-20), and tubulin (TU-02) were purchased from Santa Cruz Biotechnology Inc. The antibody for phospho-PKCζ (anti–p-PKCζ, ζ Thr410) was from Cell Signaling Technology. Anti-ubiquitin, anti-NFATc1 (NFAT2), and anti-Tak1 were provided by Vincent Chau (Pennsylvania State University College of Medicine), Nancy Rice (National Cancer Institute–Frederick, Frederick, Maryland, USA), and Jun Ninomiya-Tsuji (North Carolina State University, Raleigh, North Carolina, USA), respectively. Other antibodies have been described previously (31, 41). LPS (*E. coli* 0127:B8) and murine TNF-α were from Sigma-Aldrich and PeproTech, respectively. Recombinant M-CSF and GST-RANKL were generous gifts from Steven Teitelbaum (Washington University School of Medicine, St. Louis, Missouri, USA).

Cell line and transfection. Human embryonic kidney cell line 293T was cultured in DMEM medium with 5% FBS. The cells were seeded in 12-well plates and transfected using Lipofectamine 2000 (Invitrogen).

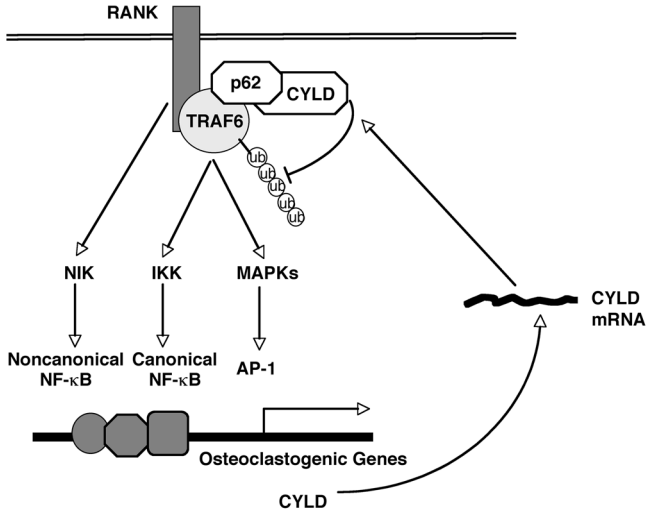

Figure 7
A model of CYLD function in RANK signaling. Engagement of RANK by RANKL induces TRAF6 ubiquitination (Ub) and activation of downstream signaling molecules, leading to induction of genes involved in osteoclastogenesis. The RANK signaling also results in upregulation of CYLD as well as p62. CYLD targets TRAF6 via the assistance of p62, thereby negatively regulating TRAF6 ubiquitination and RANK signaling.

MicroCT. Femurs of age-matched *Cyld*$^{+/+}$ and *Cyld*$^{-/-}$ male mice (14 weeks of age; 7 mice/group) were subjected to analysis by using a Scanco vivaCT 40 scanner (Scanco Medical). Distal femoral metaphysis, 263 μm–1,040 μm from the growth plate, was assessed for trabecular bone architecture. Femoral mid-diaphysis was analyzed for cortical bone morphology. Data were analyzed for statistical significance using Mann-Whitney *U* test (GraphPad Prism). A *P* value of less than 0.05 was considered significant.

Histology. Femurs of age-matched *Cyld*$^{+/+}$ and *Cyld*$^{-/-}$ male mice (14 weeks of age) were fixed in 10% neutral buffered formalin for 2 days, decalcified in 10% EDTA for 10 days, and embedded in paraffin. Sections (6 μm) were cut and subjected to H&E and TRAP staining using a TRAP assay kit (Sigma-Aldrich).

Bone marrow culture, retroviral infection, and in vitro osteoclastogenesis. BMDMs were prepared from femurs and tibia of age-matched *Cyld*$^{+/+}$ and *Cyld*$^{-/-}$ mice (4–10 weeks of age) as previously described (41). For in vitro OC differentiation, the cells were cultured in 6-well plates (1×10^6/well) in DMEM growth medium supplemented with 15–30 ng/ml M-CSF and the indicated amounts of GST-RANKL. After 4–7 days, OCs were visualized by TRAP staining using a commercial kit (Sigma-Aldrich).

Retroviral infection of bone marrow cells was essentially as described previously (41, 42) except for the use of pCL-Eco (43) as the packaging plasmid. Briefly, bone marrow cells were cultured in macrophage growth medium using 6-well plates. The cells were infected twice, on days 3 and 4, with pCLXSN(GFP) or pCLXSN(GFP)-CYLD and cultured in DMEM growth medium supplemented with M-CSF and GST-RANKL. OCs were visualized by fluorescence microscopy.

Flow cytometry. BMDMs were stained with PE-conjugated anti-mouse RANK or PE-conjugated anti-mouse M-CSFR and subjected to flow cytometry analyses as previously described (22).

IB, EMSA, and ubiquitination assay. Whole-cell lysates were prepared from BMDMs or preosteoclasts in a cell lysis buffer supplemented with phosphatase inhibitors and subjected to IB as previously described (44). Nuclear extracts were prepared and subjected to EMSA using a ^{32}P-radiolabeled oligonucleotide probes for NF-κB (5′-CAACGGCAGGGGAATTCCCCTCTCCTT-3′) and AP-1 (5′-GATCTAGTGATGAGTCAGCCG-3′).

For ubiquitination assays, cells were lysed in kinase lysis buffer supplemented with 1 mM *N*-ethylmaleimide (NEM). TRAF6 was immunoprecipitated using TRAF6-specific antibody, and the ubiquitin-conjugated TRAF6 was detected by IB using anti-ubiquitin antibody.

Real-time quantitative RT-PCR. Total RNA was isolated from preosteoclasts using TRI reagent (Molecular Research Center Inc.) and subjected to cDNA synthesis using RNase H–reverse transcriptase (Invitrogen) and oligo-dT primers. The initial quantity of cDNA samples was calculated from primer-specific standard curves with iCycler Data Analysis software. Real-time quantitative PCR was performed using iCycler Sequence Detection System (Bio-Rad) and RT^2 Real-Time SYBR green PCR master mix (SuperArray). The expression of individual genes was calculated by a standard curve method and normalized to the expression of actin for Figure 3D and GAPDH for Figure 5B. Data are presented as fold change between the RANKL-induced cells (both *Cyld*$^{+/+}$ and *Cyld*$^{-/-}$) and the unstimulated *Cyld*$^{+/+}$ cells. The gene-specific primer sets (all for murine genes) were: *Cyld*, 5′-GGACAGTACATCCAAGACCG-3′ and 5′-GAACTGCATGCGGTTGCTC-3′; TRAP, 5′-TGGTCCAGGAGCTTAACTGC-3′ and 5′-GTCAGGAGTGGGAGCCATATG-3′; cathepsin K, 5′-GTGGGTGTTCAAGTTTCTGC-3′ and 5′-GGTGAGTCTTCTTCCATAGC-3′; calcitonin receptor, 5′-CTCCAACAAGGTGCTTGGGA-3′ and 5′-GAAGCAGTAGATAGTCGCCA-3′; actin, 5′-CGTGAAAAGATGACCCAGATCA-3′ and 5′-CACAGCCTGGATGGCTACGT-3′; GAPDH, 5′-CTCATGACCACAGTCCATGCCATC-3′ and 5′-CTGCTTCACCACCTTCTTGATGTC-3′.

Acknowledgments

We thank Kang Li of the Pennsylvania State College of Medicine Core facilities for assistance with tissue sections. We thank Vincent Chau, Jun Ninomiya-Tsuji, Nancy Rice, Gregory D. Longmore, Yongwon Choi, and Steven Teitelbaum for reagents and Amgen Inc. for *Nik*-knockout mice. We also thank Valeria Facchinetti for advice on bone marrow cell infections. This study was supported by grants from the NIH (AI064639 and CA94922 to S.-C. Sun, AI057555 to S.-C. Sun and M. Zhang). All animals were housed in a facility constructed with support of a Research Facilities Improvement Grant (C06 RR-15428-01) from the National Center for Research Resources, NIH.

Received for publication October 17, 2007, and accepted in revised form February 13, 2008.

Address correspondence to: Shao-Cong Sun, Department of Immunology, The University of Texas MD Anderson Cancer Center, 7455 Fannin Street, Box 902, Houston, Texas 77030, USA. Phone: (713) 563-3218; Fax: (713) 563-3280; E-mail: ssun@mdanderson.org.

William Reiley's present address is: Trudeau Institute Inc., Saranac Lake, New York, USA.

1. Hadjidakis, D.J., and Androulakis, I. 2006. Bone remodeling. *Ann. N. Y. Acad. Sci.* **1092**:385–396.
2. Boyle, W.J., Simonet, W.S., and Lacey, D.L. 2003. Osteoclast differentiation and activation. *Nature.* **423**:337–342.
3. Teitelbaum, S.L., and Ross, F.P. 2003. Genetic regulation of osteoclast development and function. *Nat. Rev. Genet.* **4**:638–649.
4. Asagiri, M., and Takayanagi, H. 2007. The molecular understanding of osteoclast differentiation. *Bone.* **40**:251–264.
5. Takayanagi, H. 2007. Osteoimmunology: shared mechanisms and crosstalk between the immune and bone systems. *Nat. Rev. Immunol.* **7**:292–304.
6. Yamashita, T., et al. 2007. NF-kappaB p50 and p52 regulate receptor activator of NF-kappaB ligand (RANKL) and tumor necrosis factor-induced osteoclast precursor differentiation by activating c-Fos and NFATc1. *J. Biol. Chem.* **282**:18245–18253.
7. Tolar, J., Teitelbaum, S.L., and Orchard, P.J. 2004. Osteopetrosis. *N. Engl. J. Med.* **351**:2839–2849.
8. Chen, Z.J. 2005. Ubiquitin signalling in the NF-kappaB pathway. *Nat. Cell Biol.* **7**:758–765.
9. Lamothe, B., et al. 2007. Site-specific Lys-63-linked tumor necrosis factor receptor-associated factor 6 auto-ubiquitination is a critical determinant of I kappa B kinase activation. *J. Biol. Chem.* **282**:4102–4112.
10. Lamothe, B., et al. 2007. TRAF6 ubiquitin ligase is essential for RANKL signaling and osteoclast differentiation. *Biochem. Biophys. Res. Commun.* **359**:1044–1049.
11. Hacker, H., and Karin, M. 2006. Regulation and function of IKK and IKK-related kinases. *Sci. STKE.* **2006**:re13.
12. Ea, C.K., Deng, L., Xia, Z.P., Pineda, G., and Chen, Z.J. 2006. Activation of IKK by TNFalpha requires site-specific ubiquitination of RIP1 and polyubiquitin binding by NEMO. *Mol. Cell.* **22**:245–257.
13. Wu, C.J., Conze, D.B., Li, T., Srinivasula, S.M., and Ashwell, J.D. 2006. Sensing of Lys 63-linked polyubiquitination by NEMO is a key event in NF-kappaB activation. *Nat. Cell Biol.* **8**:398–406.
14. Durán, A., et al. 2004. The atypical PKC-interacting protein p62 is an important mediator of RANK-activated osteoclastogenesis. *Dev. Cell.* **6**:303–309.
15. Layfield, R., et al. 2006. p62 mutations, ubiquitin recognition and Paget's disease of bone. *Biochem. Soc. Trans.* **34**:735–737.
16. Yip, K.H., Feng, H., Pavlos, N.J., Zheng, M.H., and Xu, J. 2006. p62 ubiquitin binding-associated domain mediated the receptor activator of nuclear factor-kappaB ligand-induced osteoclast formation: a new insight into the pathogenesis of Paget's disease of bone. *Am. J. Pathol.* **169**:503–514.
17. Rea, S.L., et al. 2006. A novel mutation (K378X) in the sequestosome 1 gene associated with increased NF-kappaB signaling and Paget's disease of bone with a severe phenotype. *J. Bone Miner. Res.* **21**:1136–1145.
18. Kurihara, N., et al. 2007. Mutation of the sequestosome 1 (p62) gene increases osteoclastogenesis but does not induce Paget disease. *J. Clin. Invest.* **117**:133–142.
19. Layfield, R., and Hocking, L.J. 2004. SQSTM1 and Paget's disease of bone. *Calcif. Tissue. Int.* **75**:347–357.
20. Daroszewska, A., and Ralston, S.H. 2006. Mechanisms of disease: genetics of Paget's disease of bone and related disorders. *Nat. Clin. Pract. Rheumatol.* **2**:270–277.
21. Nijman, S.M., et al. 2005. A genomic and functional inventory of deubiquitinating enzymes. *Cell.* **123**:773–786.
22. Reiley, W.W., et al. 2006. Regulation of T cell development by the deubiquitinating enzyme CYLD. *Nat. Immunol.* **7**:411–417.
23. Jin, W., et al. 2007. Deubiquitinating enzyme CYLD regulates the peripheral development and naive phenotype maintenance of B cells. *J. Biol. Chem.* **282**:15884–15893.
24. Reiley, W.W., et al. 2007. Deubiquitinating enzyme CYLD negatively regulates the ubiquitin-dependent kinase Tak1 and prevents abnormal T cell responses. *J. Exp. Med.* **204**:1475–1485.
25. Lim, J.H., et al. 2007. Tumor suppressor CYLD regulates acute lung injury in lethal Streptococcus pneumoniae infections. *Immunity.* **27**:349–360.
26. Bignell, G.R., et al. 2000. Identification of the familial cylindromatosis tumour-suppressor gene. *Nat. Genet.* **25**:160–165.
27. Massoumi, R., Chmielarska, K., Hennecke, K., Pfeifer, A., and Fassler, R. 2006. Cyld inhibits tumor cell proliferation by blocking bcl-3-dependent NF-kappaB signaling. *Cell.* **125**:665–677.
28. Zhang, J., et al. 2006. Impaired regulation of NF-kappaB and increased susceptibility to colitis-associated tumorigenesis in CYLD-deficient mice. *J. Clin. Invest.* **116**:3042–3049.
29. Takayanagi, H., et al. 2002. Induction and activation of the transcription factor NFATc1 (NFAT2) integrate RANKL signaling in terminal differentiation of osteoclasts. *Dev. Cell.* **3**:889–901.
30. Novack, D.V., et al. 2003. The IkappaB function of NF-kappaB2 p100 controls stimulated osteoclastogenesis. *J. Exp. Med.* **198**:771–781.
31. Xiao, G., Harhaj, E.W., and Sun, S.C. 2001. NF-kappaB-inducing kinase regulates the processing of NF-kappaB2 p100. *Mol. Cell.* **7**:401–409.
32. Kovalenko, A., et al. 2003. The tumour suppressor CYLD negatively regulates NF-kappaB signalling by deubiquitination. *Nature.* **424**:801–805.
33. Sly, L.M., Rauh, M.J., Kalesnikoff, J., Song, C.H., and Krystal, G. 2004. LPS-induced upregulation of SHIP is essential for endotoxin tolerance. *Immunity.* **21**:227–239.
34. Kobayashi, K., et al. 2002. IRAK-M is a negative regulator of Toll-like receptor signaling. *Cell.* **110**:191–202.
35. Takeshita, S., et al. 2002. SHIP-deficient mice are severely osteoporotic due to increased numbers of hyper-resorptive osteoclasts. *Nat. Med.* **8**:943–949.
36. Zhou, P., et al. 2006. SHIP1 negatively regulates proliferation of osteoclast precursors via Akt-dependent alterations in D-type cyclins and p27. *J. Immunol.* **177**:8777–8784.
37. Li, H., et al. 2005. IL-1 receptor-associated kinase M is a central regulator of osteoclast differentiation and activation. *J. Exp. Med.* **201**:1169–1177.
38. Wooten, M.W., et al. 2005. The p62 scaffold regulates nerve growth factor-induced NF-kappaB activation by influencing TRAF6 polyubiquitination. *J. Biol. Chem.* **280**:35625–35629.
39. Reiley, W., Zhang, M., and Sun, S.-C. 2004. Tumor suppressor negatively regulates JNK signaling pathway downstream of TNFR members. *J. Biol. Chem.* **279**:55161–55167.
40. Reiley, W., Zhang, M., Wu, X., Graner, E., and Sun, S.-C. 2005. Regulation of the deubiquitinating enzyme CYLD by IkappaB kinase gamma-dependent phosphorylation. *Mol. Cell. Biol.* **25**:3886–3895.
41. Waterfield, M., Zhang, M., Norman, L.P., and Sun, S.C. 2003. NF-kappaB1/p105 Regulates lipopolysaccharide-stimulated MAP kinase signaling by governing the stability and function of the Tpl2 kinase. *Mol. Cell.* **11**:685–694.
42. Rivera-Walsh, I., Cvijic, M.E., Xiao, G., and Sun, S.C. 2000. The NF-kappa B signaling pathway is not required for Fas ligand gene induction but mediates protection from activation-induced cell death. *J. Biol. Chem.* **275**:25222–25230.
43. Naviaux, R.N., Costanzi, E., Haas, M., and Verma, I.M. 1996. The pCL vector system: rapid production of helper-free high-titer, recombinant retroviruses. *J. Virol.* **70**:5701–5705.
44. Uhlik, M., et al. 1998. NF-kappaB-inducing kinase and IkappaB kinase participate in human T-cell leukemia virus I Tax-mediated NF-kappaB activation. *J. Biol. Chem.* **273**:21132–21136.